Study of contact conditions at conductor/insulator interfaces used in space charge distribution measurements

Lin Zheng, Stéphane Holé

Study of contact conditions at conductor/insulator interfaces used in space charge distribution measurements

Lin Zheng and Stéphane Holé

Laboratoire de Physique et d'Étude des Matériaux (UMR 8213)

Sorbonne University – ESPCI Paris, PSL University – CNRS

10, rue Vauquelin – 75005 Paris – France

December 5, 2022

Abstract

Interfaces play a major role on charge injection in dielectrics under high voltage. As a consequence, space charge distribution measurements under high voltage may depend on the chosen interface conditions during the tests. In this paper, it is shown that various mountings of an insulating polymer (polyethylene) in a space charge distribution measurement setup develop very different intrinsic dipoles at the interfaces generating in turn an interface voltage that may interact with energy levels between the electrode and the insulator and thus with injection laws. These dipoles are minimal when the insulating polymer has hot-pressed carbon-loaded polymer electrodes or is coupled with silicone oil to carbon-loaded EVA electrodes. On the contrary aluminum coating or direct contact with aluminum in presence of silicone oil for the coupling generates large dipoles compared to gel coupling or with gold coating. The measurements were carried out with an ultra sensible pressure-wave-propagation measurement setup under very low electric field ($\pm$30 V/mm at most) for calibration purpose. Aluminum and stainless steel was used for the setup wave-guide in order to check its influence. Interface voltage up to 5 V could be estimated with an uncoated sample in contact with aluminum through silicone oil.

Keywords: space charge; interface dipole; contact potential; interface voltage; conductor/insulator interface; polymer; pressure-wave-propagation (PWP) method

Social Media Abstract: Bad choice of testing conditions may ruin insulation analysis of high voltage cables

1 Introduction

Charges that accumulate in insulating materials under high voltage, originate either from the insulator itself by molecular dissociation and migration, or from charge injection through the interfaces with adjacent materials, electrodes holding the voltage most of the time [1, 2]. As injection adds charges to the material, the charge content and buildup may reach levels well above the material withstanding. This can lead to dramatic effects such as voltage breakdown and even to the failure of the system in which the material is used. The study of charge effects in insulating materials, specially the interface effects, is therefore of particular interest.

In the conventional view of the situation [3], a charge exchange between two materials is triggered when they are brought into contact in order to reach energy equilibrium on both sides. As a consequence, a voltage appears across the interface, known as the contact potential, often associated with the difference of the energy levels (work functions) of both materials divided by the electronic charge [3, 4]. However, the interface is a break-up of the material bulk structure introducing modifications in the energy levels known as interface states that impact the contact potential [4]. This is something well studied in the case of metal/semi-conductor interfaces thanks to measurement methods relying on current-voltage characterization [4, 5]. Unfortunately, these methods cannot be used in the case of metal/insulator interfaces because there is no mobile carrier in the insulator for acting as a virtual electrode and therefore only charge barycenter could be obtained [6]. In the case of polymers, the situation is even more complex since the material structure is not totally crystalline. For instance, charge distributions in low density polyethylene (LDPE) with different electrode materials show that other processes should be considered in addition to work function and interface states . These other processes, such as polarization or the presence of residues or impurities, indeed disturb the local electric field [7, 8].

Various well known models are used to describe charge injection which depends on the actual energy barrier at the interface, and thus on the contact potential [9]. There is the Schottky effect where charges pass over the energy barrier [10], the Fowler-Nordheim effect where charges tunnel through the barrier [11], or the trap-assisted-tunneling effect where charges tunnel through the barrier to or from a trap in the insulator [12, 13]. In all cases, the energy barrier, which depends on the contact potential, is altered by the applied voltage; either lowered and/or made thinner. Therefore, current-voltage measurements can be informative though sensitive to all the interfaces encountered in the current loop during the measurements.

Until now, the effects at conductor/insulator interfaces were studied indirectly, by fitting current-voltage measurements on models [2] or by simulations [14, 15]. Extracting parameters from a model implies controlling perfectly all testing conditions, which is far from being the case when couplings or additional electrodes are necessary to perform the measurements. Indeed, all these additional layers modify the local electric field at the interface, thus deform energy levels between the electrode and the insulator, and therefore may interact with the rate charges can cross the interface [7, 8]. It is therefore of great interest to directly detect and quantify the effect of contact conditions in order to take them into account in the analysis. There were attempts to study interface effects by using space charge distribution measurements [16, 17] with the advantage of spatially separating the effects taking place at the different interfaces of the sample under test. However, the sensibility was too small to directly observe the voltage across the interface between materials. Recently, the pressure-wave-propagation (PWP) method [18, 19] has greatly improved its sensibility making it possible to observe directly the contact potential at interfaces under ultra low or zero electric field application [20, 21, 22]. The gain in sensibility of the PWP setup was made possible by an optimization of the pressure wave generator presented in Reference [23] and by using averaging. Electric fields as small as 1 V/mm on a 1-mm thick sample can be detected, which is about 100 times better than conventional setups.

In this paper, space charge distribution measurements at very low voltage were carried out to study the influence of different sample mountings. For that purpose, low density polyethylene (LDPE) with antioxidant was tested with various ways of mounting. It includes carbon-loaded-polymer electrodes (semicon) either hot-pressed or directly coupled by silicone oil or gel, or through vacuum deposited electrodes (aluminum or gold). In the following section, samples, measurement setup and measurement protocol are presented. The calibration technique and how the information is obtained are also

described. In the last section before conclusion, measurements are shown, analyzed and discussed.

2 Samples, set-up and protocol

2.1 Samples

Samples were taken from the same high voltage low-density-polyethylene specimen (see Figure 1). The high voltage specimen contains antioxidant and is 20-cm diameter and 1-mm thick and has two 5-cm-diameter 0.5-mm thick carbon-loaded polyethylene hot-pressed on both sides. Because the study is under low voltage, the high voltage specimen was cut into various 3-cm-diameter samples. This ensures that the insulating polymer samples studied in this paper have very similar chemical composition since they have been extracted from the same specimen and thus have been made at the same time in the same conditions. Nine samples were cut out from the high voltage specimen, one in the center having then two hot-pressed carbon-loaded polyethylene electrodes on both sides, and height in the periphery being then free of electrodes. From these 8 latter samples, two have been coated under vacuum with aluminum electrodes on both sides, two have been coated under vacuum with gold electrodes on both sides, and the last four remained uncoated, thus without electrodes. In addition, carbon-loaded Ethylene Vinyl Acetate (EVA) electrodes, 1 mm in thickness, were coupled either with silicone oil or gel (Sofranel gel D) to all samples except the one having hot pressed electrodes. It was then possible to test 7 sample mountings with two different couplings.

2.2 Measurement set-up

The pressure-wave-propagation (PWP) method [24] is a well suited space charge distribution measurement method for studying interfaces. Compared to the other measurement methods [18], it does not induce intrinsic signals at the interfaces that mask the effect of interest such as in the case of the pulsed electro-acoustic (PEA) method. Moreover, it allows the various interfaces of the sample to be well distinguished thanks to elastic wave propagation instead of heat diffusion as in thermal methods. The principle of the PWP method is illustrated in Figure 2. A pressure pulse is transmitted to the sample to test. During the propagation, the charges encountered are displaced resulting in an electric current in the circuit connecting the electrodes of the sample. Because the pressure pulse propagates at the velocity of sound, the current generated at a given time corresponds to the charge displaced at the position of the pressure pulse at that time. As a consequence, the current profile is an image of the charge distribution inside the sample and the charge position can be deduced by the time at which the signal appeared multiplied by the velocity of sound.

In the case of the present work, the pressure pulses were generated by a piezoelectric generator [21] made of a 15-mm-diameter 0.2-mm-thick Pz24 piezoelectric ceramic from Meggitt stuck by epoxy resin with a 3-cm-long brass backing on one side and a 2-cm-long aluminum wave-guide on the other side. As this structure has a derivative response [23], 380-V voltage steps were applied every 20 ms, generating one pressure pulse every 20 ms. The sample, acoustically coupled to the wave-guide on one side and pressed by 0.5 bar with a brass counter electrode on the other side, could be stressed by a voltage through a 5-kΩ resistor. The generated signal was decoupled from the stress voltage by a 880 nF capacitor and then amplified by a 66-dB HCA-10M-100K FEMTO amplifier. The signal was finally acquired and averaged by a MSO44 Tektronix scope. A picture of the setup is shown in Figure 3.

Although less efficient, a stainless steel wave-guide was also used to evaluate the possible interactions between the aluminum wave-guide and the couplings and their influence in the signal. With 7 sample mountings, 2 different couplings and 2 different wave-guides, there were finally 28 different situations evaluated.

2.3 Measurement protocol

Prior to any measurements, the samples were cured at 80°C under short-circuit for 7 days in order to relax the residual charges that could have been present or injected for instance by triboelectricity during the cutting, the cleaning or the coating. When the samples were mounted in the measurement setup, a first measurement was carried out under short-circuit, then under positive voltages up to +30 V, under short-circuit again, under negative voltage down to −30 V, and finally under short-circuit. All measurements were averaged 1024 times. The flowchart in Figure 4 illustrates the sample preparation (in blue) and measurement protocol (in green).

2.4 Calibration and analysis technique

The expression of the signal $i(t)$ in short-circuit measurement conditions for a planar sample is [25]

$$i(t) = -C_0 \int (1 - a/\epsilon)\, E(x)\, \frac{\partial S(x,t)}{\partial t}\, \mathrm{d}x, \tag{1}$$

where C_0 is the capacitance at rest of the sample, a its electrostrictive coefficient and ϵ its permittivity. In this expression, x is the position in depth, t is time, $E(x)$ is the electric field distribution and $S(x,t)$ is the strain wave. As the insulating polymer can be considered uniform in the scope of this study, a and ϵ can get out of the integral. In addition, the strain being the derivative over space of the local material displacement, one has $\partial S/\partial t = \partial V/\partial x$, where $V(x,t)$ is the particle velocity, in other words the speed at which matter is locally displaced due to the pressure wave. It is worth noting that pressure and particle velocity are proportional together and the coefficient of proportionality is the acoustic impedance [26]. Therefore, the shape of the particle velocity is the same as the one of the pressure pulse.Using Gauss-Maxwell equation to make charge density $\rho(x)$ appear and after an integration by parts, it comes

$$i(t) = \kappa \int \rho(x)\, V(x,t)\, \mathrm{d}x, \tag{2}$$

where $\kappa = A\,(1 - a/\epsilon)/d$, A is the sample area and d its thickness. Expression (2) explicitly shows that the measured current $i(t)$ originates from the charges that are displaced at particle velocity V. Providing a sample free of internal charges and since charges are not expected to buildup in the sample under very low electric field, at most 30 V/mm in the present study, it can be assumed that charges are present only at the interfaces on very small extent compared to the pressure pulse extent. As a consequence, for a charge density $\rho(x) = \sigma\,\delta(x - x_0)$ confined at the interface $x = x_0$, with $\delta(x)$ the Dirac function, one obtains from (2) the signal

$$i_\sigma(t) = \kappa\,\sigma\, V(x = x_0, t) \tag{3}$$

which is proportional to the surface charge density σ at $x = x_0$ and to the particle velocity $V(x = x_0, t)$ at that interface. This situation is illustrated in Figure 5a. Induced charges due to the voltage application generate such signal peaks. For an applied voltage V_{app}, one would obtain the calibration signal $i_{cal}(t)$

at the first interface ($x_0 = 0$ which is ground electrode)

$$i_{cal}(t) = -\kappa\,\epsilon\,\frac{V_{app}}{d}\,V(x=0,t) \tag{4}$$

with d the sample thickness.

In presence of a surface dipole density $\vec{\pi} = \sigma\delta\vec{\ell}$ at $x = x_0$, the signal is the superposition of a signal generated first by the negative charge $-\sigma$ of the dipole and second by the positive charge $+\sigma$ of the dipole. The delay between these two signals is $\delta\ell/v_s$, where v_s is the speed of sound, hence the overall current is

$$\begin{aligned} i_\pi(t) &= -i_\sigma(t+\frac{\delta\ell}{2v_s}) + i_\sigma(t-\frac{\delta\ell}{2v_s}) \approx -\frac{\partial i_\sigma(t)}{\partial t}\,\frac{\delta\ell}{v_s} \\ &\approx -\kappa\,\sigma\,\frac{\partial V(x=x_0,t)}{\partial t}\,\frac{\delta\ell}{v_s} = -\frac{\kappa\,\pi}{v_s}\,\frac{\partial V(x=x_0,t)}{\partial t}. \end{aligned} \tag{5}$$

This signal has a bipolar shape and is proportional to the surface dipole density π. This is illustrated in Figure 5b.

The integral over time of $i_\pi(t)$ is proportional to the particle velocity at the interface and can be directly compared to the calibration signal $i_{cal}(t)$. As a consequence

$$\int i_\pi(t)\,\mathrm{d}t = -\frac{\kappa\,\pi}{v_s}\,V(x=x_0,t) = \frac{d}{v_s\,V_{app}}\,\frac{\pi}{\epsilon}\,i_{cal}(t) \tag{6}$$

so the (algebraic) peak amplitude of the integral over time of $i_\pi(t)$ divided by the (algebraic) peak amplitude of $i_{cal}(t)$ gives a constant from which the dipole surface density π and thus the interface voltage or contact potential π/ϵ can be determined by:

$$\frac{\pi}{\epsilon} = \frac{v_s\,V_{app}}{d}\,\frac{\mathrm{peak}\,(\int i_\pi(t)\,\mathrm{d}t)}{\mathrm{peak}\,(i_{cal}(t))}, \tag{7}$$

where $\mathrm{peak}(s(t))$ denotes the algebraic peak amplitude of the signal $s(t)$. It is worth noting that $v_s\,V_{app}/d$ corresponds to the ratio of the applied voltage during calibration with transit time of the pressure pulse through the sample. The transit time can be directly obtained from the calibration measurement since it exhibits two peaks, a first one due to the charges on the electrode at the first interface and a second one due to the charges on the electrode at the second interface. The delay between these two peaks is therefore the time for the pressure pulse to travel through the sample, thus the transit time by definition. This factor is therefore easy to extract from measurements without introducing other source of errors. It is also worth noting that peak amplitudes can be confidently used as long as attenuation and dispersion are negligible or if peaks are taken at the same position. Otherwise, the peak surface should be taken instead in order to get rid of this uncertainty.

3 Results and discussion

3.1 Detailed analysis of a typical signal

Figure 6 presents three typical raw signals for the hot-pressed sample coupled with gel to the aluminum wave-guide, one under short-circuit (green curve), one with back electrode held to +30 V (red curve)

and the last with back electrode held to -30 V (blue curve). The acquired raw signals appear in millivolts which correspond to the measured current $i(t)$ multiplied by the gain of the amplifier and its 50-Ω-input impedance (see Figure 2). As the ratio in (7) cancels these coefficients, the acquired signals are shown in their raw units, thus millivolts. The front electrode is always connected to ground through the wave-guide. All signals show a bipolar peak when the pressure arrives at the interface between the aluminum wave-guide and the front electrode. This corresponds to the dipole induced by the coupling gel that may have reacted with the aluminum of the wave-guide [27]. This bipolar peak, which begins at 3.13 μs since the wave-guide is 20-mm thick, can be modeled by (5). Then an unipolar peak, negative under $+30$ V and positive under -30 V, is generated at 3.37 μs when the pressure arrives at the interface between the front electrode and the insulating polymer. This corresponds to the charges, negative under $+30$ V and positive under -30 V, induced by the applied voltage on the ground electrode and can be modeled by (3). Finally an unipolar peak, positive under $+30$ V and negative under -30 V, is generated at 3.80 μs when the pressure reaches the interface between the insulating polymer and the back electrode. This corresponds to the charges, positive under $+30$ V and negative under -30 V, induced by the applied voltage on the back electrode and can also be modeled by (3).

A combined signal depending only on the applied voltage can be easily calculated for instance from half the difference of the signal under $+30$ V and the one under -30 V. This signal combination is used thereafter as the calibration signal which is necessary to obtain the required information for the interface voltage estimation (see signal processing part in red in Figure 4). In a similar way, a combined signal independent of the applied voltage can be calculated for instance from half the sum of the signal under $+30$ V and the one under -30 V. This latter combination should correspond to the signal under short-circuit which is useful for a double check of experimental results. These combined signals are shown in Figure 7a and their integration over time in Figure 7b. Because noise is present in the measurements, calculated interface voltage are given thereafter within an interval of confidence ($\pm$ sign) corresponding to the standard deviation of the estimation. From (7), one obtains a voltage at the wave-guide interface of -879 ± 104 mV and -825 ± 98 mV when taking peak surface instead of peak amplitude. A negative voltage means that wave-guide is positively charged compared to carbon loaded electrode. These results are similar considering their interval of confidence, which means that attenuation and dispersion through the carbon loaded electrode have little influence in this example. Peak surface is used thereafter to get rid of slight differences in peak shape. As there is no detectable signal at the interfaces of the insulating polymer under short-circuit, the voltage at these interfaces can be estimated lower than 100 mV which corresponds more or less to the limit of detection.

Notice that integration over time of the voltage dependent combined signal does not go back to zero at the back side, *i.e.* $A_2 \neq 0$ (see blue curve in Figure 7b). In fact, hot-pressed electrodes do not perfectly mechanically match the insulating polymer. The pressure wave reflection at the back side of the insulator then lowers the peak. If the sample is assumed symmetrical, this brings information on the matching at the interface between the front electrode and the insulator. Figure 8 describes the effects of partial reflections at each interface. The ratio of the levels of the integrated signal after (A_2) and before (A_1) the back electrode peak gives directly the refection coefficient Γ_2 of the pressure at the back interface, here $\Gamma_2 = A_2/A_1 = 0.12$. The signal at the back interface is therefore $1 - \Gamma_2 = 0.88$ folds the one at the front interface of the insulator. Hence, due to the assumed sample symmetry which leads to $\Gamma_1 = -\Gamma_2$, the signal at front interface is itself $1 + \Gamma_2 = 1.12$ folds the one at the interface between the wave-guide and the front electrode. As a consequence, the former results for the voltage at the wave-guide interface should be divided by 1.12 leading to -738 ± 88 mV.

3.2 Other results

Compared to aqueous gel, silicone oil increases the intrinsic voltage at the wave-guide interface up to -3010 ± 117 mV and an induced dipole of -17 ± 1 mV/V superimposes. The induced dipole and the applied electric field are in the same direction (from back electrode to front electrode). This is conventional for oil polarization in electric field and is certainly due to a non-perfect electrical contact between carbon loaded polyethylene and aluminum wave-guide. When a stainless steel wave-guide is used, the voltage at the wave-guide interface drastically reduces to -458 ± 307 mV and -487 ± 157 mV respectively for gel and oil and there is no longer induced dipole detected. It can thus be assumed that aluminum of the wave-guide has a great influence on the interface voltage, probably due to chemical reactions [27] with the coupling media with a much larger impact of oil than gel. On the contrary, a wave-guide made of a more inert material produces lower effects, relatively similar for oil and gel, which may be attributed to the coupling.

In the figures presented now on, all measurements have been corrected from calibration and amplitudes are expressed in Volt per square microseconds. Assuming the shape of the bipolar peak as the convolution of a decreasing exponential with the derivative of a Gaussian pulse, the interface voltage can be roughly estimated by

$$0.846 A_1 \tau_1^2 \left(1 - \frac{A_1}{A_2}\right) \left(-\frac{A_1}{A_2} - 0.6\right)^{0.1}, \tag{8}$$

where τ_1 is the width at mid amplitude of the first part of the bipolar peak and A_1 and A_2 are the algebraic amplitudes of the first and second parts of the bipolar peak; A_1 and A_2 are obviously of opposite polarity. Estimations given in the text are however directly calculated from the measurements and are thus more accurate and intervals of confidence can be evaluated. It is worth noting that curves are similar to charge profiles except that amplitudes are opposite. Thus positive charges appear as a negative signal and negative charges appear as a positive signal. This is due to the minus in $\vec{E} = -\vec{\text{grad}}(V)$.

Though cable manufacturers co-extrude insulation with carbon loaded electrodes in order to obtain a well defined contact [28], many tests are carried out without such a close contact only made possible by co-extrusion or hot-pressing. Instead, carbon loaded polymer layers, for instance EVA, are coupled to the insulting polymer under test. In Figure 9, the combined signals independent to applied voltage are shown, corrected from setup efficiency thanks to the calibration signal. A 1-mm-thick EVA electrode is inserted on both sides of the insulating polymer and gel or oil is used as acoustic coupling. The insulating polymer is either aluminum coated, gold coated or left uncoated. In all cases, aluminum-coated sample presents the larger dipole at the insulating interface, *i.e.* 1474 ± 262 mV with gel and 2347 ± 188 mV with oil. The lower dipole at the insulator interface is obtained by the gold-coated sample when using gel ($+521 \pm 256$ mV) whereas it is obtained without coating when using oil (almost undetectable).

Although all signals at the wave-guide interface should be similar for gel or for oil, it is clear that charge exchange exists across EVA electrode. When aluminum is present on both sides of the EVA layer, the dipole is large on both sides with gel or oil. However, with gold-coated or uncoated samples, the dipole at the wave-guide interface is quite similar and the dipole at the insulator interface is much smaller with oil. This points to the great impact of aluminum and, to a smaller extent, of gel for uncoated sample. The use of a stainless steel wave-guide (see Figure 10) gives similar results except that dipoles at the wave-guide interface are mush smaller than with an aluminum wave-guide.

A direct contact of the sample with the wave-guide exposes the signal to more perturbation since it is no longer possible to dissociate the coupling impact on the wave-guide and on the insulating polymer. In Figure 11a, the contact is made through gel. Whatever the coating of the insulating polymer, a quite large dipole appears at the interface with the wave-guide. It corresponds to a voltage at the interface of $+282 \pm 87$ mV for the aluminum-coated insulator, -121 ± 28 mV for the gold-coated insulator and $+350 \pm 59$ mV for the uncoated insulator. Notice that voltage at the interface is opposite (wave-guide charges negatively compared to insulator) for aluminum-coated and uncoated insulator compared to previous situations. Notice also the asymmetry of the bipolar peak of the gold-coated insulator indicating a possible competition between two dipoles, one between gel and the aluminum of the wave-guide, and one between gel and the gold-coated insulating polymer. As a consequence the estimated dipole may in fact be not well calculated.

When using oil instead of gel, the voltage at the interface changes drastically only for uncoated sample since one obtains -5023 ± 252 mV, therefore a large increase in amplitude and a polarity reversal. When stainless steel is used for the wave-guide instead of aluminum, similar behavior is observed with gel (see Figure 12a) in terms of shape and amplitude considering the lower sensitivity of the stainless steel setup. The counter dipole due to the aluminum of the wave-guide in case of gold-coated sample is however more visible since one peak is visible and delayed at the interface. This can be explained by a compensation of the bipolar signals as sketched in the inset of Figure 12a. This indicate actually an intrinsic effect of gold with the insulating polymer. Using oil, (see Figure 12b) the effects are similar than with the aluminum wave-guide for aluminum or gold coated insulating polymer showing more the impact of the coating than the one of the wave-guide. As to the uncoated polymer, the voltage at the interface is still reversed but the amplitude is reduced by a factor 3.

3.3 Discussion

From all results, a clear voltage appears at the interfaces in all cases except when carbon loaded polymer electrodes are hot-pressed on the insulating polymer, and, to a lower extent, when carbon-loaded EVA is directly coupled through silicone oil to the uncoated insulating polymer. Aluminum has a great impact on the voltage at the interfaces, larger for silicone oil than for aqueous gel. This is visible at the aluminum wave-guide interface or at aluminum coated electrodes. The use of a stainless steel wave-guide reduces the effect compared to an aluminum wave-guide but not cancels them.

Gold coating has a different behavior than aluminum. Indeed, though the dipole appearing at the interface with the insulating polymer is clearly almost symmetrical in terms of shape for any other contacts, the contact with gold present a sharp peak on gold side and a much broader peak inside the insulator. Both peaks have more or less the same surface which is compatible with a dipole, but this points out that charges clearly spread inside the polymer with gold-coating contrarily to aluminum-coated or uncoated polymer. Figure 13 shows it clearly and, though the amplitude slightly changes depending on the material the gold-coated polymer is coupled to, the shape is rather similar. As the broader peak in the polymer is much larger than spatial resolution, this is significant. This could be explained by the diffusion of charges inside the insulator according to a kind of Debye length. Hence it can be assumed that charges are blocked at the interface for aluminum and uncoated polymer, whereas they can much more easily drift in the polymer with gold coating. Furthermore, as gold is positively polarized compared to the insulating polymer when using oil whereas it is negatively polarized when using gel, both positive and negative charges could drift. This show the impact of the coupling on the interface prop-

erties. It is worth noting that 5-nm thick chromium is deposited on the surface of the polymer before gold to improve adhesion. In addition, by thoroughly analyzing measurements with gold electrodes, one observes that it starts slightly after the others, as if a preceding (in the course of the measurement) counter dipole would have existed. A sketch of these dipoles is shown in dashed lines superimposed to the signals in Figure 13. The assumed dipole due to the sample is positive with gel and negative and twice as much with oil. The assumed dipole due to the coupling seems to be always negative with a much larger amplitude in case of direct contact with the aluminum wave-guide. Stainless steel greatly reduces the influence of aluminum without completely canceling the influence of the wave-guide.

4 Conclusion

It is clearly demonstrated that interface effects may drastically vary from one measurement condition to another. Measurements show the appearance of intrinsic dipoles at the interface that generate interface voltages. The potential distribution at the interface, and thus the energy levels, is then modified which may interact directly with different charge injection processes or threshold when the structure will be subjected to high voltage. Hot-pressed carbon loaded electrode presents negligible interface voltage.

As it is known that coupling material can polarize under voltage, one would have expected that metallized polymers should be better than uncoated polymers. However, it is shown in the results that a carbon-loaded EVA electrodes coupled through silicone oil to an uncoated polymer generate a smaller interface voltage than when the polymer is aluminum coated or gold coated. On the contrary, a coupling directly on aluminum generates a very large interface voltage and in that case, gel may be better. It has been emphasis that aluminum generates in all cases a large interface voltage. The uses of stainless steel reduces the impact without canceling it. Last but not least, gold-coating seems to ease charge spreading in the polymer.

This study points to the great impact of interface conditions that must be well defined and well controlled in the study of space charges in materials. Indeed, they can result to different behaviors as those expected and thus to dramatic situation if test conditions are not representative to operating conditions. The use of a high sensitive pressure-wave-propagation (PWP) setup makes it possible to study interface phenomena. Though physical effects were mainly considered at interface in the case of dielectric insulation, chemical reactions should also be considered.

References

[1] R. Coelho. *Physics of Dielectrics for the Engineer*. Elsevier, 1979. ISBN: 0-444-41755-9.

[2] J.C. Fothergill and L.A. Dissado. *Space Charge in Solid Dielectrics*. The Dielectric Society, 1992. ISBN: 0 9533538 0 X.

[3] C. Kittel. *Introduction to Solid State Physics*. John Wiley & Sons, Inc, 2005. ISBN: 0-471-41526-X.

[4] S.M. Sze. *Semiconductor devices: physics and technology*. John Wiley & Sons, USA, 2001. ISBN: 0471333727.

[5] E.H. Nicollian and J.R. Brews. *MOS (Metal Oxide Semiconductor) physics and technology*. John Wiley & Sons, USA, 1982. ISBN: 0471085006.

[6] X. Zhang and G.M. Sessler. Charge transport in silicon nitride/silicon oxide double layers. In *11th International Symposium on Electrets (ISE 11)*, pages 122–125, Melbourne, Autralia, 2002.

[7] M. Taleb, G. Teyssedre, S. Le Roy, and C. Laurent. Modeling of charge injection and extraction in a metal/polymer interface through an exponential distribution of surface states. *IEEE Transactions on Dielectrics and Electrical Insulation*, 20:311–320, 2013. DOI: 10.1109/TDEI.2013.6451372.

[8] Kai Wu and Chuanhui Cheng. Interface charges between insulating materials. *IEEE Transactions on Dielectrics and Electrical Insulation*, 24:2633–2642, 2017. DOI: 10.1109/TDEI.2017.006442.

[9] F. Neumann, Y. A. Genenko, C. Melzer, S. V. Yampolskii, and H. von Seggern. Self-consistent analytical solution of a problem of charge-carrier injection at a conductor/insulator interface. *Phys. Rev. B*, 75:205322, 2007. DOI: 10.1103/PhysRevB.75.205322.

[10] J.G. Simmons. Richardson-Schottky effect in solids. *Phys. Rev. Lett.*, 15:967–968, 1965. DOI: 10.1103/PhysRevLett.15.967.

[11] R.H. Fowler and L. Nordheim. Electron emission in intense electric fields. *Proc. R. Soc. Lond. A*, 119:173–181, 1928. DOI: 10.1098/rspa.1928.0091.

[12] N. Gaillard. *Etude des Propriétés Morphologiques, Electriques et Chimiques de l'Interface Métal/Isolant et de leur Impact sur les Performances de la Capacité TiN/Ta_2O_5/TiN*. Phd thesis, Université Joseph Fourier Grenoble I, December 2006. available at https://tel.archives-ouvertes.fr/tel-00142484/file/N.Gaillard-These.pdf.

[13] G. Papaioannou, F. Coccetti, and R. Plana. On the modeling of dielectric charging in RF-MEMS capacitive switches. In *2010 Topical Meeting on Silicon Monolithic Integrated Circuits in RF Systems (SiRF)*, pages 108–111, 2010. DOI: 10.1109/SMIC.2010.5422970.

[14] F. Boufayed, S. Leroy, G. Teyssedre, C. Laurent, P. Segur, L.A. Dissado, and G.C. Montanari. Simulation of bipolar charge transport in polyethylene featuring trapping and hopping conduction through an exponential distribution of traps. In *International Symposium on Electrical Insulating Materials (ISEIM)*, volume 2, pages 340–343, 2005. DOI: 10.1109/ISEIM.2005.193557.

[15] R. Guffond, A. Combessis, and S. Hole. Polymer electrical property simulation using genetic model. In *2018 ieee 2nd international conference on dielectrics, icd 2018*, page 8468403, 2018. DOI: 10.1109/ICD.2018.8468403.

[16] P. Morin, C. Alquié, and J. Lewiner. Correlation between space charge distributions and external current measurements during the discharge of low density polyethylene samples. In *8th International Symposium on Electrets (ISE8)*, pages 265–270, NJ, USA, 1994. IEEE. DOI: 10.1109/ISE.1994.514779.

[17] J.C. Fothergill, L.A. Dissado, J. Alison, and A. See. Advanced pulsed electro-acoustic system for space charge measurement. In *8th International Conference on Dielectric Materials*, pages 352–356, IEE Conf. Publ. No. 473, 2000. DOI: 10.1049/cp:20000532.

[18] S. Holé, T. Ditchi, and J. Lewiner. Non-destructive methods for space charge distribution measurements: what are the differences? *IEEE Trans. Dielectr. EI.*, 10:670–677, 2003. DOI: 10.1109/TDEI.2003.1219652.

[19] J. Lewiner, S. Hole, and T. Ditchi. Pressure wave propagation methods: a rich history and a bright future. *IEEE Transactions on Dielectrics and Electrical Insulation*, 12(1):114–126, 2005.

[20] S. Holé. Contact potential measurement at metal/insulator interface. In *2019 IEEE International Symposium on Electrets (ISE17)*, page 51, Limerick, Ireland, September 2019.

[21] A. Ndour, S. Holé, P. Leblanc, and T. Paillat. Direct observation of electric charges at solid/liquid interfaces with the pressure-wave-propagation method. *Journal of Electrostatics*, 109:103527, 2021. DOI: 10.1016/j.elstat.2020.103527.

[22] L. Zheng and S. Holé. Space charge measurement under very low voltage for assessing interface effects due to measurement conditions. In *4nd International Conference on Dielectrics, ICD2022*, pages 2b–9, Palerm, Italy, July 2022.

[23] S. Holé and J. Lewiner. Design and optimization of unipolar pressure pulse generators with a single transducer. *J. Acoust. Soc. Am.*, 104:2790–2797, 1998. DOI: 10.1121/1.423863.

[24] P. Laurenceau, J. Ball, G. Dreyfus, and J. Lewiner. Une méthode nouvelle de détermination de la distribution spatiale des potentiels dans les diélectriques. *C. R. Acad. Sc. Paris*, 283:135–138, 1976.

[25] S. Holé, T. Ditchi, and J. Lewiner. Influence of divergent fields on space charge distribution measurements using elastic methods. *Phys. Rev. B*, 61:13528–13539, 2000. DOI: 10.1103/PhysRevB.61.13528. In Eq. (21) B_k should be E_k and in Eq. (47) ϵ_j should be ξ_j.

[26] P. M. Morse and K. U. Ingard. *Theoretical acoustics*. McGraw-Hill Inc, New York, U.S.A., 1968. ASIN: 070433305.

[27] C. Vargel. *Corrosion of aluminium*. Elsevier, 2020. ISBN: 9780080999258.

[28] W. R. Kegerise. Manufacturing and performance criteria for medium voltage power cable semiconducting shields. *IEEE Electrical Insulation Magazine*, 24:15–21, 2008. DOI: 10.1109/MEI.2008.4473050.

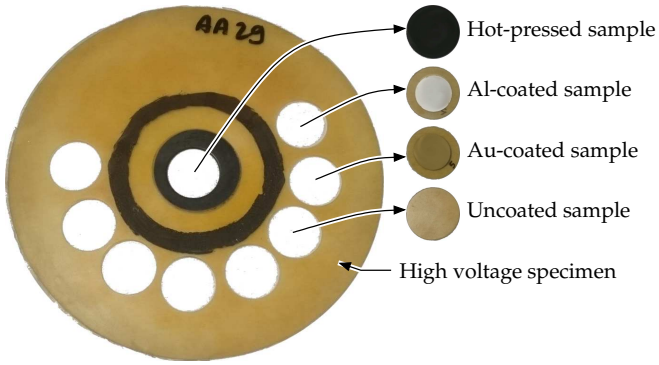

Figure 1: Original high voltage specimen from which 3-cm-diameter samples were cut out. The high voltage specimen is made of a 1-mm-thick 20-cm-diameter polyethylene disk including antioxidant on which 5-cm-diameter 0.5-mm-thick carbon loaded polyethylene electrode were hot-pressed stuck on both sides in the middle of the disk. The sample taken from the middle has got hot-pressed electrodes. Samples taken from the periphery were coated with aluminum electrodes, gold electrodes, or left without electrodes (uncoated).

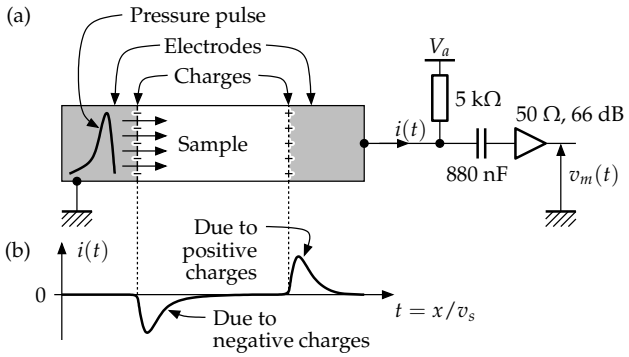

Figure 2: Pressure-wave-propagation principle. (a) A pressure pulse is transmitted to the sample under test. It displaces the charges one after another at the velocity of sound v_s generating a current $i(t)$ at (b) the image of the charge distribution.

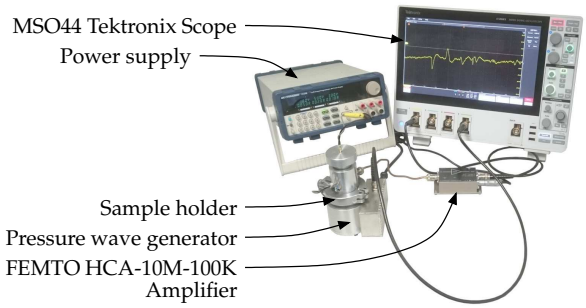

Figure 3: Picture of a PWP setup used for low voltage measurements.

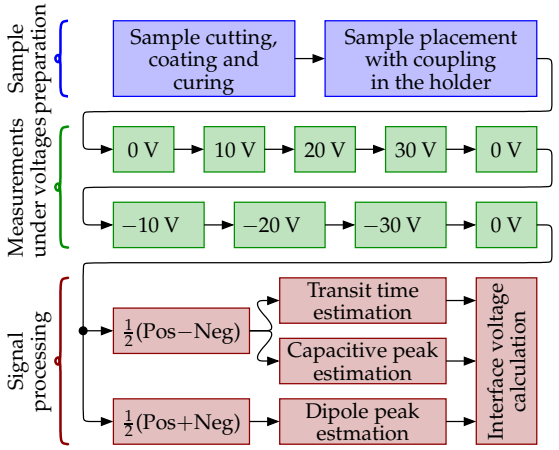

Figure 4: Flowchart of the measurement protocol from the sample preparation to the interface voltage determination. Half the difference of measurements under positive and negative voltages of the same amplitude is referred to as $\frac{1}{2}(\mathrm{Pos}-\mathrm{Neg})$ and half the sum of measurements under positive and negative voltages of the same amplitude is referred to as $\frac{1}{2}(\mathrm{Pos}+\mathrm{Neg})$.

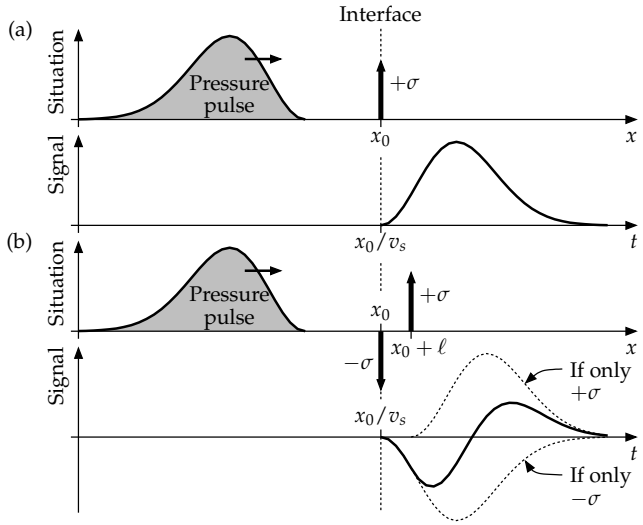

Figure 5: Illustration of the signal produced by a pressure pulse. (a) In case of a single surface charge $+\sigma$ located at x_0, the signal starts at x_0/v_s and is proportional to σ and to the pressure pulse. (b) In case of a surface dipole $\sigma\ell$ which negative charge $-\sigma$ is located at x_0 and positive charge $+\sigma$ at $x_0+\ell$, the signal also starts at x_0/v_s and is proportional to $\sigma\ell$ and to the pressure pulse derivative over time. In dotted lines, the signals that would have been produced if only one of the dipole surface charge were present.

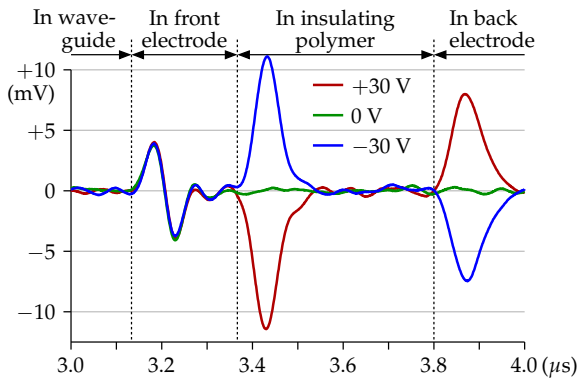

Figure 6: Typical signals for the hot-pressed sample under different voltages. A voltage independent bipolar peak is detected at the interface between wave-guide and front electrode and voltage dependent unipolar peaks are detected at the interfaces between the insulator and its electrodes. Dotted lines indicate when the pressure begins to cross an interface.

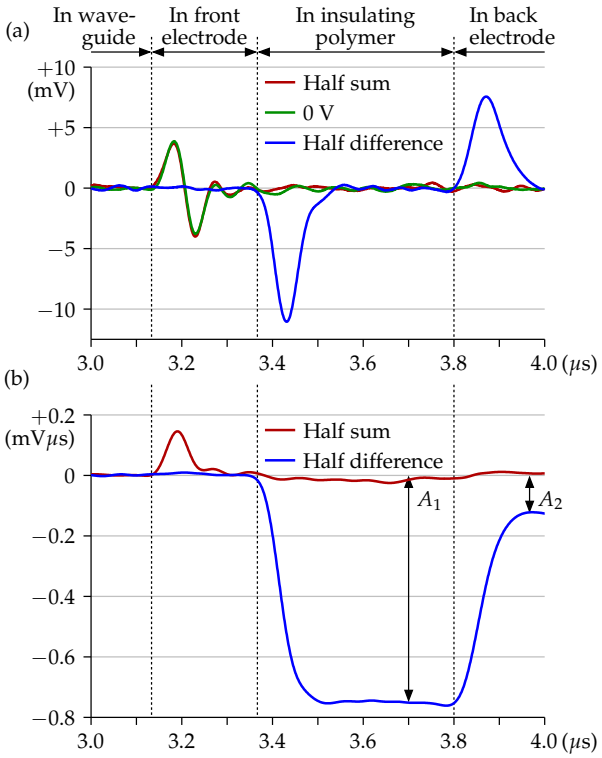

Figure 7: (a) Typical combined signals for the hot-pressed sample. This allows to evidence what depends or not on the applied voltage. (b) integration over time of the combined signals. Dotted lines indicate when the pressure begins to cross an interface.

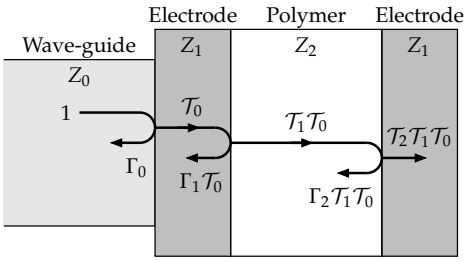

Figure 8: Pressure wave amplitude at the various interfaces. Material displacement and pressure are continuous at an interface but the pressure wave is modified from one interface to another due impedance mismatches. Here Z stands for the acoustic impedance, Γ for the pressure-wave reflection coefficient and $\mathcal{T}$ for the pressure-wave transmission coefficient.

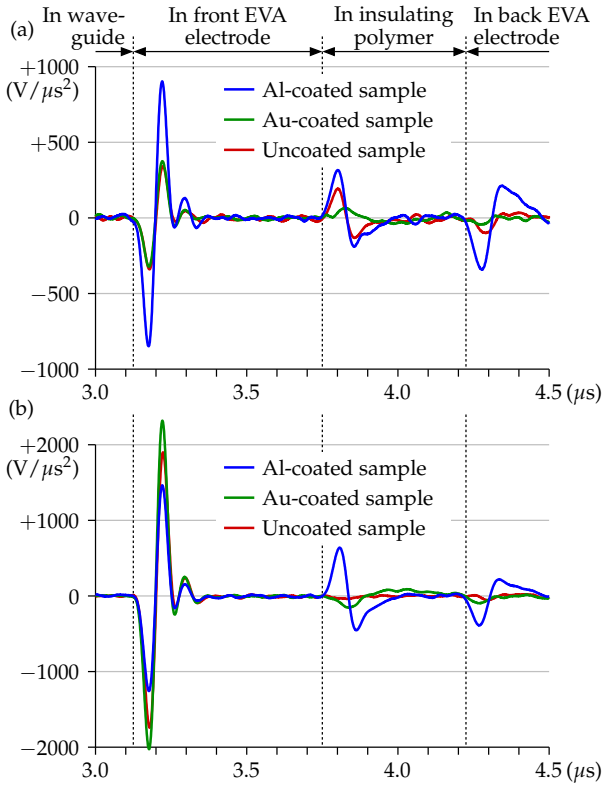

Figure 9: Calibrated combined signals independent to applied voltage with samples coupled to 1-mm thick EVA electrode either (a) with gel or (b) with silicone oil. Samples are aluminum coated, gold coated of left uncoated and tested in the aluminum-wave-guide setup. A double integration over time of each bipolar peak gives the voltage at the corresponding interface. Dotted lines indicate when the pressure begins to cross an interface.

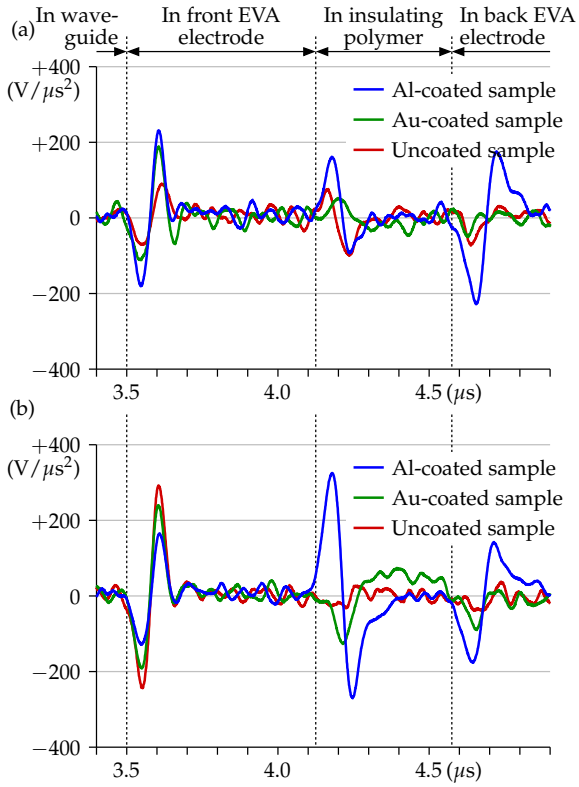

Figure 10: Calibrated combined signals independent to applied voltage with samples coupled to 1-mm thick EVA electrode either (a) with gel or (b) with silicone oil. Samples are aluminum coated, gold coated of left uncoated and tested in the stainless steel wave-guide setup. A double integration over time of each bipolar peak gives the voltage at the corresponding interface. Dotted lines indicate when the pressure begins to cross an interface.

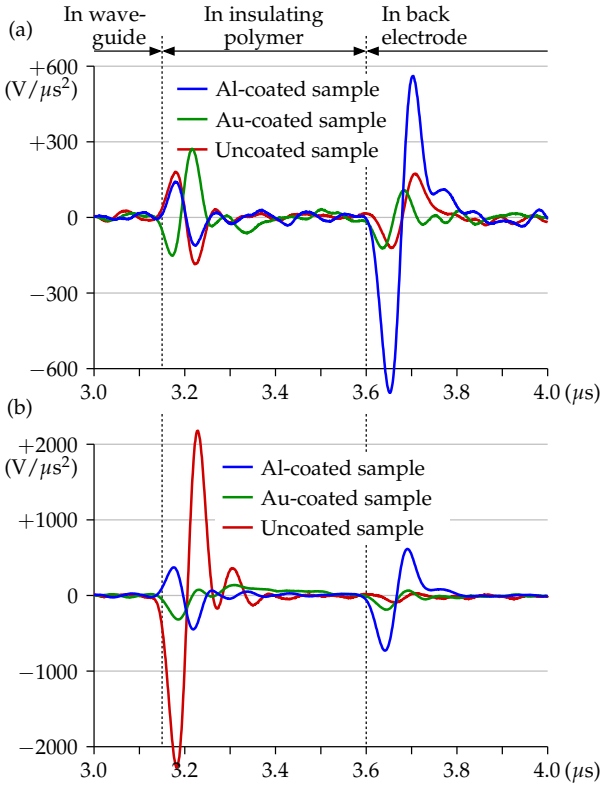

Figure 11: Calibrated combined signals independent to applied voltage with samples directly coupled either (a) with gel or (b) with silicone oil to the aluminum wave-guide of the setup. Samples are aluminum coated, gold coated of left uncoated. A double integration over time of each bipolar peak gives the voltage at the corresponding interface. Dotted lines indicate when the pressure begins to cross an interface.

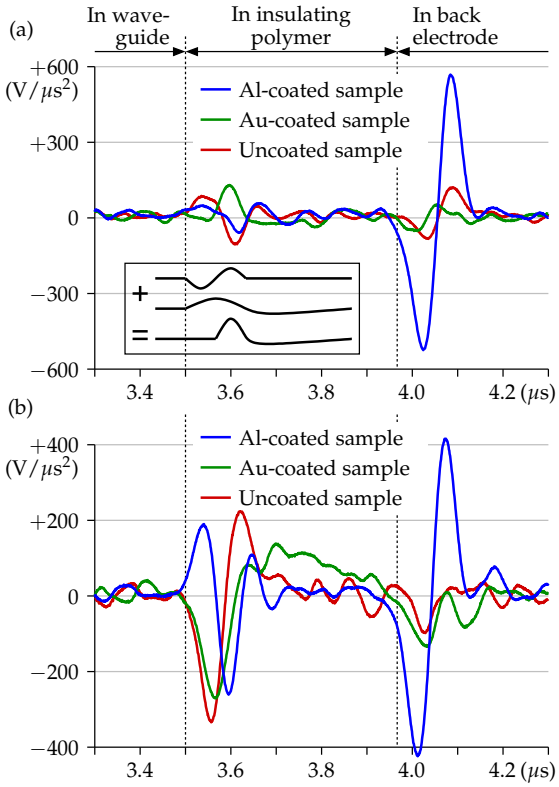

Figure 12: Calibrated combined signals independent to applied voltage with samples directly coupled either (a) with gel or (b) with silicone oil to the stainless steel wave-guide of the setup. Samples are aluminum coated, gold coated of left uncoated. A double integration over time of each bipolar peak gives the voltage at the corresponding interface. Dotted lines indicate when the pressure begins to cross an interface. In the inset, a possible explanation of the delay for gold signal with gel using the superposition of two dipoles.

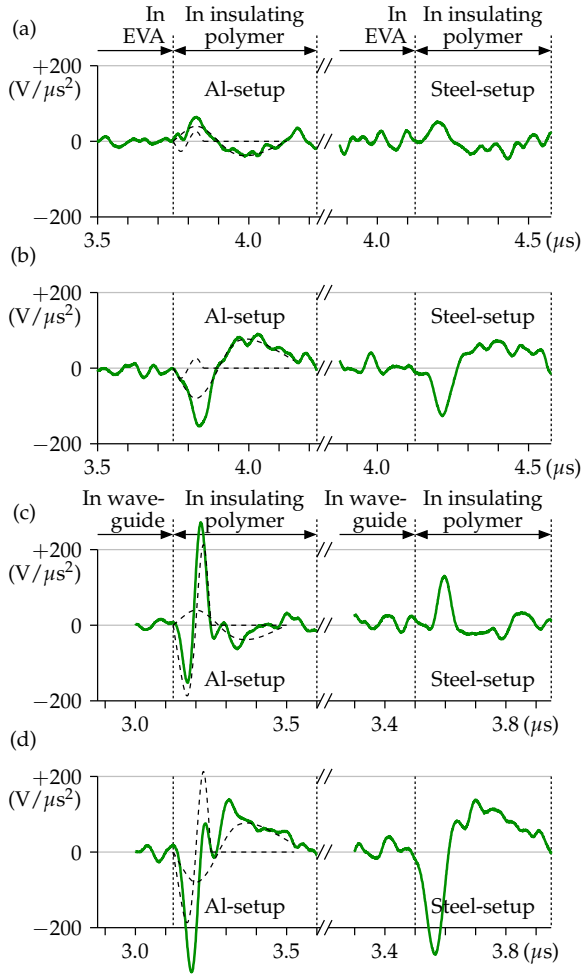

Figure 13: Calibrated combined signals independent to applied voltage with gold-coated sample in aluminum setup (left) or stainless-steel setup (right). (a) Sample coupled through gel to carbon-loaded EVA. (b) Sample coupled through oil to carbon-loaded EVA. (c) Sample coupled through gel to the wave-guide. (d) Sample coupled through oil to the wave-guide. Dotted lines indicate when the pressure begins to cross an interface.